Palaeogeography, Palaeoclimatology, Palaeoecology 568 (2021) 110294

Contents lists available at ScienceDirect

Palaeogeography, Palaeoclimatology, Palaeoecology

journal homepage: www.elsevier.com/locate/palaeo

Mercury record of intense hydrothermal activity during the early Cambrian, South China

Guangyou Zhu [a,*], Pengju Wang [a], Tingting Li [a], Kun Zhao [b], Wang Zheng [c], Xinbin Feng [d], Jun Shen [e], Stephen E. Grasby [f], Guangyi Sun [d], Shunlin Tang [g], Huihui Yan [a]

[a] Research Institute of Petroleum Exploration and Development, PetroChina, Beijing 100083, China
[b] State Key Laboratory of Oil and Gas Reservoir Geology and Exploitation & Institute of Sedimentary Geology, Chengdu University of Technology, Chengdu 610059, China
[c] Institute of Surface-Earth System Science, School of Earth System Science, Tianjin University, Tianjin 300072, China
[d] State Key Laboratory of Environmental Geochemistry, Institute of Geochemistry, Chinese Academy of Sciences, Guiyang 550081, China
[e] State Key Laboratory of Geological Processes and Mineral Resources, China University of Geosciences, Wuhan, Hubei 430074, China
[f] Geological Survey of Canada, Natural Resources Canada, 3303 33rd Street NW, Calgary, Alberta T2L 2A7, Canada
[g] Institute of Resources and Environment, Henan Polytechnic University, Henan 454000, China

ARTICLE INFO

Keywords:
Mercury isotopes
Ocean anoxia
Hydrothermal activity
Total organic content

ABSTRACT

The early Cambrian was an important interval in Earth history, marked by significant evolution of both life and the marine environments it inhabited. While enhanced hydrothermal activity has been proposed as a trigger for ecosystem perturbations in the early Cambrian, it remains unclear how intense and how long such perturbations may have been. To address this, we examined mercury (Hg) concentrations and mercury isotopes, as well as major and trace elements, of organic-rich black shales of the lower Cambrian Niutitang Formation, in the Tongren area of Guizhou Province, South China. Our data show that Hg in these sediments is hosted dominantly by organic matter. Elevated raw and normalized Hg contents provide direct evidence of intense hydrothermal activity during the early Cambrian in South China. We suggest that high metal flux (e.g., Mo, U, and Ba) into the seawater occurred through this intense submarine volcanism, altering seawater compositions. Intense hydrothermal activity was likely a significant trigger of environmental and biological evolution during the early Cambrian in South China.

1. Introduction

The Ediacaran-Cambrian (E-C) transition was one of the most important periods in Earth history (Shu et al., 2014). During this period, dramatic changes occurred to ocean geochemistry during a time also marked by rapid biological evolution (Knoll and Carroll, 1999). The E-C transition is most notably characterized by a significant decline in the Ediacaran mollusk population (Narbonne, 2005), and subsequent emergence of small shell fauna (Knoll and Carroll, 1999; Zhu, 2010). During the early Cambrian, evolution occurred at the level of phylum, and most of the existing modern phyla emerged at that time (Knoll and Carroll, 1999). This biological evolution is closely related to the evolution of the marine environment (e.g., trace metal and oxygen concentration in seawater) (Anbar and Knoll, 2002; Li et al., 2017). Study of the early Cambrian can thus provide crucial insight into these co-evolution processes. Insight into these processes also has important economic implications as they form some of the most important hydrocarbon source rocks in the world (Zhu et al., 2015).

Submarine volcanism has been assumed to have had significant control on the chemical composition and oxygen concentration of seawater during the early Cambrian, even leading to mineralization of the seafloor (Baross and Hoffman, 1985; Perner et al., 2013). The hydrothermal metal flux is also thought to have altered the chemical composition of seawater (Chen et al., 2009); while at the same time hydrothermal vent systems provided habitat for biological communities (Baross and Hoffman, 1985; Mcdermott et al., 2015). Thus, studies on seafloor hydrothermal activity can provide insight into the linkage of geological processes driving geochemical cycles, that have influenced the origin and evolution of life (Baross and Hoffman, 1985).

Although submarine volcanism is assumed to be the trigger for

* Corresponding author.
E-mail address: zhuguangyou@petrochina.com.cn (G. Zhu).

https://doi.org/10.1016/j.palaeo.2021.110294
Received 24 September 2020; Received in revised form 6 February 2021; Accepted 7 February 2021
Available online 23 February 2021

marine environmental perturbations that influenced biological evolution during the early Cambrian, direct evidence of hydrothermal activity is lacking (Zhou and Jiang, 2009; Och et al., 2015). For example, while the mineralization of the polymetallic Ni-Mo-PGE has been studied for decades, many different hypotheses were proposed to explain these, mainly including seawater purification (Lehmann et al., 2007) and submarine hydrothermal eruption (Jiang et al., 2006; Guo et al., 2016). To address the lack of direct evidence for volcanism, we examined mercury concentrations and its isotopes, as a fingerprint of volcanic eruptions. While widely used to reconstruct the ancient continental as well as submarine volcanism throughout Earth history (Sanei et al., 2012; Grasby et al., 2017, 2019), mercury, and especially mercury isotope, are rare in the early Cambrian (Yin et al., 2017; Faggetter et al., 2019; Shen et al., 2020).

Volcanogenic emissions are the dominant natural source of Hg to the surface environment in pre- anthropocene time. Hg emissions are mainly in the form of gaseous elemental mercury—Hg(0), accounting for more than 90% of the total geogenic Hg in the modern atmosphere (Selin, 2009). The residence time of Hg(0) in the atmosphere is about 6 months to 2 years, allowing for long distance transport and atmospheric mixing (Blum et al., 2014). Hg(0) can be oxidized to Hg(II), which is more soluble in water than Hg(0) and is easily transferred from the atmosphere to oceans by dry or wet deposition (Selin, 2009). In addition, mercury can also be transported to the marine environment by terrigenous inputs (such as clay and organic matter) carried by rivers (Grasby et al., 2017; Them et al., 2019). In the marine environment, mercury exists in the form of elemental mercury ($Hg(0)_{aq}$), divalent inorganic mercury ($Hg(II)_{aq}$), methyl mercury (Me-Hg) and mercury compounds bound to particles (HgP_{aq}) (Selin, 2009). In seawater $Hg(II)_{aq}$ can be reduced to Hg(0) and released into the atmosphere. It can also be removed into sediments by adsorption onto suspended particles in the water column (Selin, 2009), which is usually proportional to primary productivity (Ravichandran, 2004). Most HgP_{aq} is released back into the water during the process of organic matter remineralization. Only a minor fraction of HgP_{aq} reaches the deep sea and accumulates in sediments (Ravichandran, 2004). In marine sediments, mercury tends to form strong and stable complex compounds with organic matter and reduced sulfur (Ravichandran, 2004). Besides organic matter, sulfides, and clay minerals are also important hosts for Hg in sediments (Grasby et al., 2019; Them et al., 2019; Shen et al., 2019a, 2020).

Mercury isotope fractionation especially mass independent fractionation (MIF) is considered to be an effective indicator of the origin and transformation of mercury (Blum et al., 2014). Photochemical reaction (such as photoreduction of Hg(II) or photodegradation of methyl mercury) (Zheng and Hintelmann, 2010) is the main mechanism of mercury MIF (Blum et al., 2014). Therefore, MIF is commonly used to reflect the source or environmental processes related to photochemistry. In general, marine materials (sediments and organisms) tend to show positive MIF, while terrestrial sources (including coal, soil, sediments, and plants) tend to present negative MIF due to accumulation of atmospheric Hg(0) (Yin et al., 2016). In addition, The MIF of volcanic mercury is close to zero ($+0.02 \pm 0.06‰$; Yin et al., 2016). During periods of major volcanic activity, mercury concentration could be enriched in marine sediments, accompanied by significant changes in mercury MIF, providing a fingerprint for the origin of mercury enrichment (Grasby et al., 2017, 2019, 2020; Shen et al., 2019b). Mercury concentrations as well as MIF are widely used as a promising volcanic proxy in ancient sediments (Grasby et al., 2019). Previous work has also examined Hg contents and its isotope to understand the source of metal enrichment in the early Cambrian Niutitang black shale from the west of Guiyang, South China (Fig. 1, Yin et al., 2017), which suggested that metal enrichment is related to high bioproductivity and Hg scavenging.

In our study, Hg concentration and stable isotopes were analyzed from an outcrop profile at Songtao County in Tongren, Guizhou Province. Our aim was to explore the records of hydrothermal activity and its effect on the oceanic environmental perturbations during the early Cambrian.

2. Geological background and study sections

The South China Craton is composed of the Yangtze Block and the Cathaysia Block (Wang, 1985). The Nanhua Basin, formed between these two blocks, and was connected with the open ocean during the early Cambrian (Jin et al., 2016). During the early Cambrian, the South China Block was an independent craton at mid-latitudes of the northern hemisphere (Fig. 1A), with about 80° counterclockwise rotation relative to its modern location (Li et al., 2008). The sedimentary successions of the early Cambrian are well preserved, and three sedimentary facies are developed successively from the northwest to the southeast: 1) the littoral facies; 2) the Yangtze shallow water carbonate shelf facies, and 3) the slop-basin facies (Fig. 1B) (Steiner et al., 2007). The shallow-water carbonate-platform facies mainly consists of dolomites, and intercalated limestone and phosphorous rocks. The slope facies are mainly shale/mudstones of the lower member of the Niutitang Formation. The basinal facies are dominated by cherts and shale. In the Tongren area the early Cambrian Niutitang Formation is mainly a thick black mudstone to shale, with interbeds of mudstone and argillaceous siltstone in its lower part (0 to 18.76 m). The middle part (18.76–36.96 m) is mainly characterized by silty mudstone, occasionally with calcareous mudstone intercalations. The upper part (36.96–57.16 m) is mainly composed of mudstone with thin layers of calcareous mudstone. In this study, we focus on the black mudstone in the lower part of the Niutitang Formation (Fig. 2A).

The study section (Wuluo) belongs to the slope setting, where the

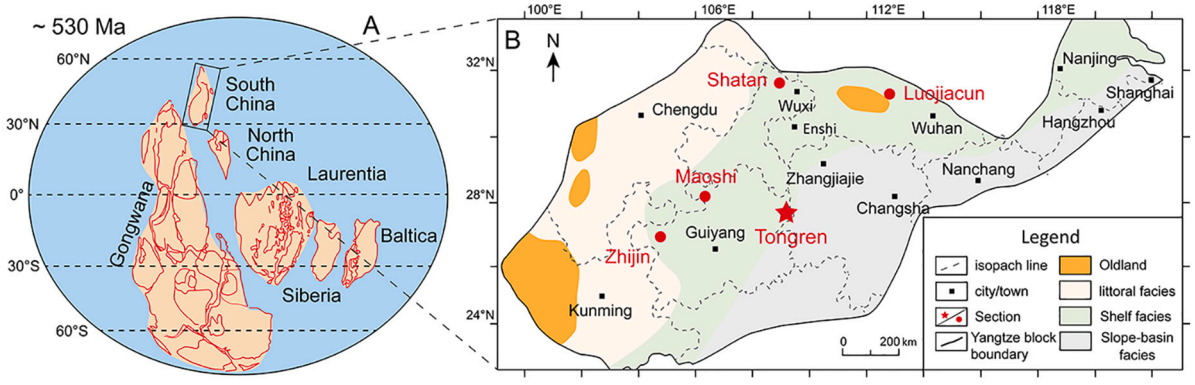

Fig. 1. (A) Global paleogeographic map for early Cambrian (~530 Ma) (modified after Li et al., 2008). (B) Early Cambrian paleogeographic map of the South China Craton (Wang, 1985). The red circles represent previous study areas, including: Zhijin (Yin et al., 2017), Maoshi (Yin et al., 2017), Luojiacun (Shen et al., 2020), and Shatan (Shen et al., 2020). (For interpretation of the references to color in this figure legend, the reader is referred to the web version of this article.)

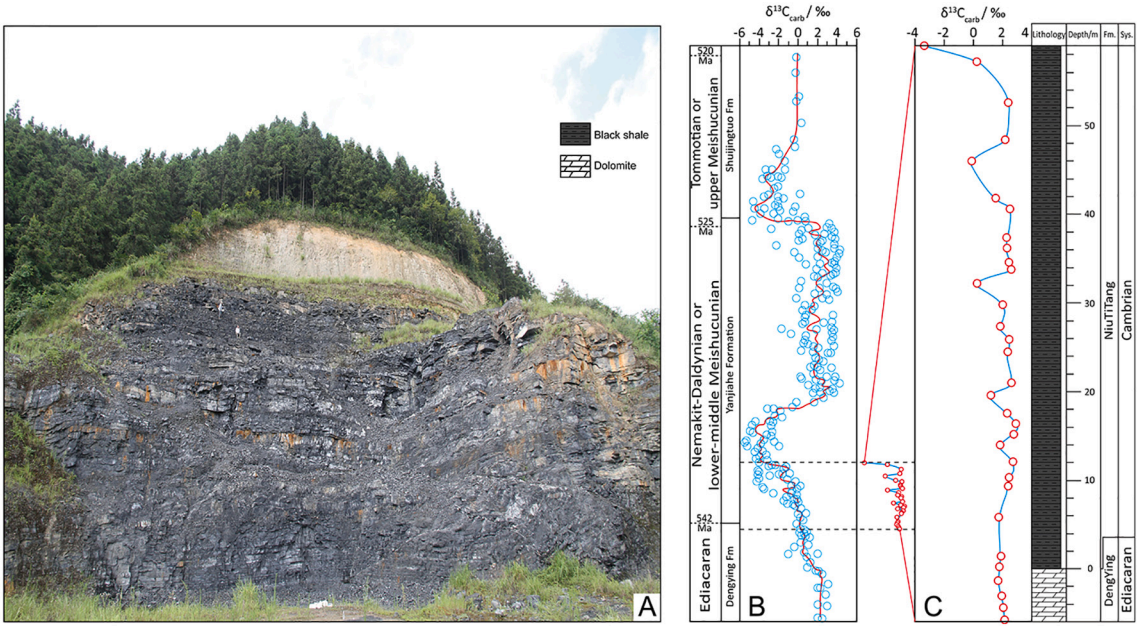

Fig. 2. (A) Field photo of the study section. (B) Carbonate carbon isotopic distribution curve in the Ediacaran-Cambrian in South China (cited from Jiang et al., 2012). (C) Carbonate carbon isotopes in the studied section. FM. = Formation; Sys. = System.

Niutitang Formation uncomfortably overlies the dolomites of the Ediacaran Dengying Formation, similar to the other sections in South China. While at deep-water basin facies, the carbonate dominated Dengying Formation transitions to the chert and shale dominated Liuchapo Formation. At the study section, the lower part (~59 m) of the Niutitang Formation is well exposed due to surface mining activity (Fig. 2A). According to zircon U—Pb geochronology and carbon isotope profiles, the Ediacaran-Cambrian boundary is within the Liuchapo Formation (Chen et al., 2015). Thus, the Niutitang Formation belongs to the early Cambrian, and the age at its base is 522 to 524 Ma (Bowring et al., 2007; Wang et al., 2012; Chen et al., 2015). Generally, the Niutitang Formation is correlative with the shallow water Shuijingtuo Formation. The negative carbon isotope shift in our data also locates our studied interval as the earliest Cambrian, as it is consistent with the carbon isotope characteristics of the lower Cambrian in the Three Gorges area (Jiang et al., 2012) (Fig. 2B-2C).

3. Samples and methods

We collected 130 fresh samples from the study section and removed all the weathered surface to ensure accurate results. These samples were used for comprehensive measurements of total organic carbon (TOC) (130 samples), Hg (120 samples), Hg isotopes (35 samples), major and trace elements (36 samples), as well as total sulfur concentrations (30 samples). All samples were prepared as powders before analysis. TOC was analyzed using a Leco CS-200 carbon–sulfur analyzer. The samples were first treated with 10% HCl to remove carbonates, and then washed with distilled water to remove HCl, and dried before analysis.

Hg contents of the samples were determined by Lumex RA-915 M. About 100 mg sample powder was placed in the sample vessel of PYRO-915+. Then, the powder was heated to 680–740 °C under pyrolysis, so that all forms of mercury in the sample are converted into elemental mercury. With a RA-915 M analyzer, the generated elemental mercury contents were quantitatively determined on basis of the absorption of 254 nm co-amplitude radiation by the mercury atomic vapor. The detection limit is 0.5–1 ppb. Duplicates were measured for each sample (relative standard deviation ≤5%). The international standard sample NIST 1633c Coal Fly Ash (1005 ± 22 ppb) was used for generation of the standard curve ($R^2 \geq 0.999$) and quality control, and a standard was measured every 10 samples to monitor for drift.

A subset of samples were chosen for mercury (Hg) isotope measurement by MC-ICP-MS at the State Key Laboratory of Environmental Geochemistry, Institute of Geochemistry, Chinese Academy of Sciences. The samples were pre-concentrated into 5 mL of a 40% mixed acid solution (v/v, $3HNO_3/1HCl$) using a double-stage combustion protocol for Hg isotope analysis as previously described (Huang et al., 2016). NIST-3133 Hg standard and secondary standard solutions (UM-Almadén and NIST-3177) were prepared to match the Hg concentrations and matrix of sample solutions within 10%. The specific data are shown in Supplementary Table 1, and the calculation formula is as follows:

$$\delta^{X}Hg(‰) = \left[\left({}^{X}Hg/{}^{198}Hg\right)_{Sample} \Big/ \left({}^{X}Hg/{}^{198}Hg\right)_{standard} - 1\right] \times 1000 \quad (1)$$

where X represents the mass number of Hg isotopes between ^{199}Hg and ^{202}Hg. MIF ($\Delta^{X}Hg$) is calculated as follows:

$$\Delta^{X}Hg = \delta^{X}Hg - \beta \times \delta^{202}Hg \quad (2)$$

where X represents the mass numbers of Hg isotope, which is 199, 200 and 201 respectively. β is a scaling factor used for correcting theoretical MDF fractionation. The β values of ^{199}Hg, ^{200}Hg and ^{201}Hg is 0.2520, 0.5024 and 0.7520, respectively.

The UM-Almadén standard and NIST 3177 were used to determine the analytical accuracy of the isotopic analyses, and the isotopic ratios of $\delta^{202}Hg$, $\Delta^{199}Hg$, $\Delta^{200}Hg$, and $\Delta^{201}Hg$ were similar to previously reported values). Data uncertainties (±2σ) reported here reflect the larger values of either the external precision of the replication of the standard solutions (UM-Almadén, NIST 3177 and GSS-4) or sample replicates.

Elemental analyses for major, trace and rare earth elements were carried out using inductively coupled plasma–mass spectrometry (ICP–MS), which is equipped with a Finnigan MAT Element 1 mass spectrometer (Finnigan MAT, San Jose, California) at the Beijing Institute of Nuclear Industrial Geology. About 40 mg of powder from each sample was digested with 0.5 mL diluted HNO_3 (i.e., analytically pure HNO_3 mixed with water at a volume ratio of 1:1) and 1 mL HF in a Teflon® digestion vessel, and then processed by ultrasonic vibration for 10–15 min. The Teflon digestion vessel was then placed on an electrical heating plate at about 150 °C for 7 to 10 days to remove all silica. After that, the residue was mixed with 2.0 mL of HNO_3 until it was completely

dissolved using the ICP-MS. Analytical accuracy was estimated to be better than 5%.

Samples for carbonate carbon isotope analyses were analyzed in the Petroleum Geology Laboratory, China University of Petroleum. Each sample was cut into two or more chips in order to avoid any weathered surface. Sample powders were drilled from clean or polished slabs and were then used for analyses. Isotopic results are expressed in the standard notation as per mil (‰) deviation from VPDB. Approximately 50–200 μg carbonate powder was reacted with orthophosphoric acid for 10 min at 70 °C in a Kiel IV carbonate device automatically connected to a Finnigan Delta Plus dual-inlet mass spectrometer. Analytical uncertainties determined by duplicate measurements of NBS-19 and an internal standard are better than 0.1‰.

4. Results

Mercury (Hg) concentrations in mudstone samples range from 1.0 to 623 ppb, with an average of 143 ppb (Fig. 3A). Hg concentrations decrease from the Lower Member (LM, 0 to 30 m, average value is 193 ppb) to the Upper Member (UM, 30 to 59 m, average value is 63 ppb). The TOC content ranges from 0.2 to 5.1 wt%, with an average of 1.4 wt% (Fig. 3B). TOC and Hg exhibit similar fluctuations, over three cycles. The Hg/TOC ratios range from 14.6 to 602 ppb/wt%, with an average of 106 ppb/wt% (Fig. 3C). They are higher in the LM (ranging from 35.4 ppb/wt% to 602 ppb/wt%, average of 143 ppb/wt%), and decrease in the UM (ranging from 14.6 ppb/wt% to 282 ppb/wt%, average of 45.7 ppb/wt%) of the study section.

Mass-independent fractionation (MIF, Δ^{199}Hg) values range from −0.18‰ to +0.21‰, with a mean value of +0.03 ± 0.03‰ (n = 35) (Fig. 3D). MIF values are higher in the LM (> −0.05‰), and lower in the UM (≤0.05‰). Mass-dependent fractionations (MDF, δ^{202}Hg) values are between −4.03‰ and − 0.78‰ (Fig. 3E), averaging −2.45 ± 0.35‰ (2SD). MDF show a trend that mirrors the MIF values, with lower values in the LM (≤2‰), but higher values in the UM (≥2‰).

The Eu anomalies (Eu/Eu*) range from 1 to 2 for most of samples in the section, but higher values (>3) are exhibited in the middle part of the LM (Fig. 3F). The enrichment factor (EF) of trace elements (Cu, Ni, U, Mo, and Ba) are high in the study section (Fig. 3G). Ba Mo, U show extreme enrichment (e.g. EF > 10), and Cu, Ni exhibit intermediate to slight enrichments (EF <10). Generally, all the trace elements (TE) show higher and lower EFs in the LM, and UM respectively. Ratios of TE to TOC are similar to the EFs of TE, exhibiting higher values in the LM, and lower values in the UM (Fig. 3H).

5. Discussion

5.1. Mercury host in marine sediments

In marine sediments, mercury can exist in various components such as organic matter, clay minerals and sulfide (Ravichandran, 2004; Sanei et al., 2012; Grasby et al., 2019; Shen et al., 2019a, 2020). As organic matter is generally considered as the principal host for mercury in marine sediments, mainly in the form of organic-mercury complex (Ravichandran, 2004; Grasby et al., 2019), TOC is widely used to normalize Hg to account for the effect of changes in organic matter deposition on Hg concentration. However, Hg has high affinity to sulfide as well, making sulfide minerals the main phase of mercury sequestration under euxinic conditions (Sanei et al., 2012; Grasby et al., 2019; Shen et al., 2019a). Besides organic matter and sulfides, clay minerals which can adsorb Hg(II) due to large surface areas and high charges, are also important hosts for Hg in sediments, although in lesser amounts than organic matter and sulfides (Grasby et al., 2019; Shen et al., 2020).

Mercury is dominantly associated with organic matter in our samples. Firstly, Hg and TOC show similar profiles, yielding relatively higher (e.g. >200 ppb and >4 wt% for Hg and TOC) and lower (e.g. <200 ppb and <4 wt% for Hg and TOC) values in the LM and UM, respectively (Figs. 3A and B). Secondly, Hg and TOC exhibit much higher correlation coefficients ($r = +0.77$, $p < 0.01$, $n = 125$) than Hg and TS ($r = +0.32$, $p > 0.05$, $n = 27$) or Hg and Al ($r = +0.67$, $p < 0.01$, $n = 35$) (Fig. 4A-C). The total sulfur (TS) content of the studied sediments is low (most of the samples are <1.0 wt% in TS contents and TOC/TS ratios are <0.35). These can be compared to the statistical threshold values of TS > wt.1% and TS/TOC > 0.35, as well as TS < 1 wt% or TS/TOC < 0.35 for sulfide hosted and organic matter hosted Hg in sediments, respectively (Shen et al., 2020). Mercury hosted by organic matter were also reported in other low TS early Cambrian sediments in South China (Shen et al., 2020). In summary, normalization of Hg concentrations to TOC is appropriate as organic matter is the main host phase in the present study.

5.2. Redox effects on Hg deposition

The Hg content of modern marine sediments is commonly influenced by various environmental factors including redox condition, organic

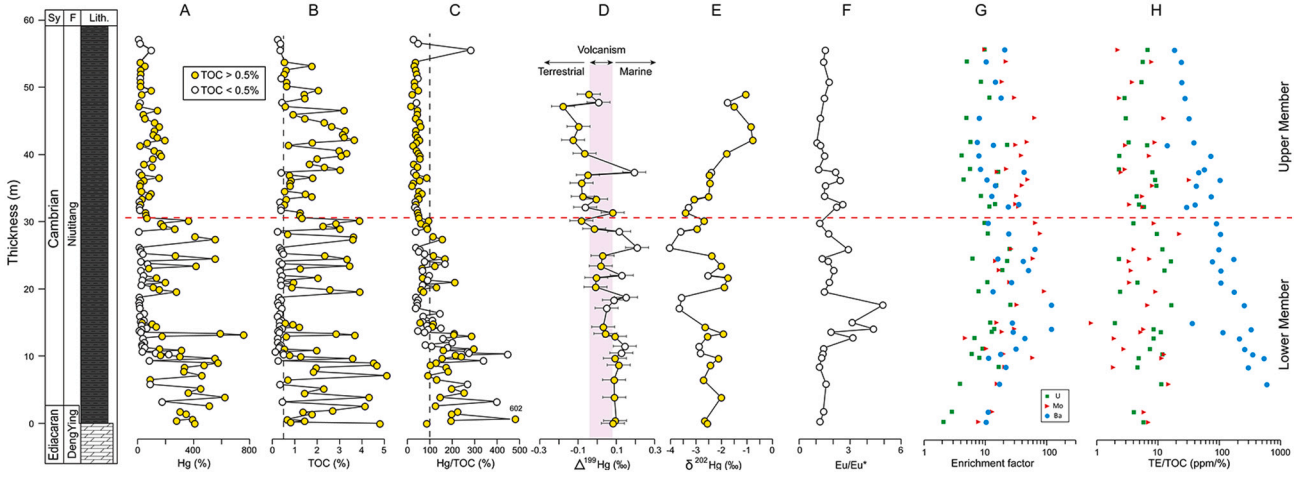

Fig. 3. Profiles of: (A) mercury (Hg) concentration (ppb); (B) total organic carbon (TOC) concentration (wt%); (C) ratios of Hg to TOC (ppb/wt%); (D) mass-independent fractionation (Δ^{199}Hg, ‰); (E) mass-dependent fractionation (δ^{202}Hg, ‰); (F) Eu anomalies (Eu/Eu*); (G) enrichment factor of trace elements; and (H) ratios of trace elements to TOC (ppm/wt%). Eu/Eu* was calculated as $2Eu_N/(Sm_N + Gd_N)$. The subscript "N" indicates normalization to post-Archean average shale (PAAS; Taylor and McLennan, 1985). The shaded rectangle in column D is the background values of volcanic Δ^{199}Hg (+0.02 ± 0.06‰, Yin et al., 2016), and it's a rough interpretation, not absolute.

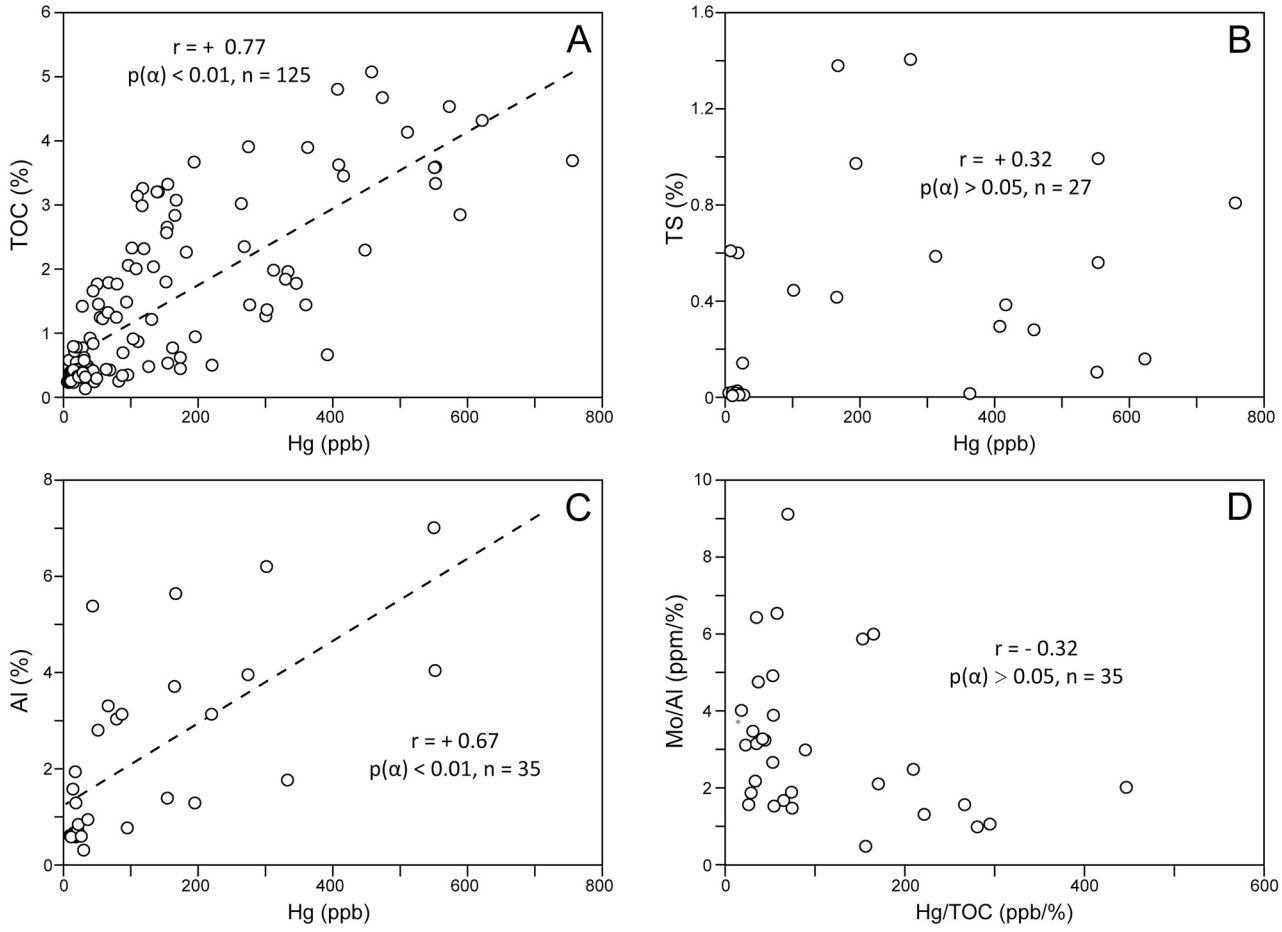

Fig. 4. Cross plots of: (A) TOC and Hg; (B) TS and Hg; (C) Al and Hg; and (D) Mo/Al and Hg/TOC. *r* represents the positive (+), and negative (−) correlation coefficient. The number in the bracket (behind comma) represent the number of samples. Refer to the web version for interpretation of the color.

carbon burial flux, and clay mineral deposition (Ravichandran, 2004). Redox conditions are considered as a key factor affecting sequestration of mercury from seawater to marine sediments (Ravichandran, 2004). Reducing conditions facilitate the preservation of organic matter and the formation of Hg—OM complexes (Ravichandran, 2004). Reducing conditions are also favorable for the formation of HgS and the absorption of Hg by iron sulfide (Sanei et al., 2012; Grasby et al., 2019; Shen et al., 2019a).

In our study, redox conditions exert negligible control on mercury content. The redox conditions are suboxic to anoxic for samples with lower TS and TS/TOC values as mentioned above. The relative lower concentrations of redox sensitive trace elements (e.g. U and Mo) in the section, as compared to modern anoxic/euxinic sediments (Algeo and Tribovillard, 2009), further support limited removal of these metals by reducing conditions (Fig. 3F). Similar U and Mo values are reported in other sections from South China indicating that these are more regional conditions (e.g. Liu et al., 2018). The negative correlations between Hg/TOC and Mo/Al ($r = -0.32$) further support changing redox conditions having a negligible effect on enhanced Hg sequestration (Fig. 4D).

5.3. Submarine volcanic sources of Hg in sediments

Elevated raw and normalized Hg (Hg/TOC) data suggest additional Hg was delivered to the early Cambrian oceans. High Hg/TOC in this study cannot be the result of the calculation errors caused by low TOC content, as most of the TOC values are >0.5% at the higher Hg/TOC intervals (e.g., LM). While such mercury enrichments in sediment are seen as indicators for Hg depositional events during numerous critical intervals, such as mass extinction and oceanic anoxia events, they are not always definitive of volcanic eruptions (Grasby et al., 2019). Stable isotope data can provide further insight into the source of Hg (e.g. Grasby et al., 2017, 2019).

Mass-independent fractionation of mercury isotopes (MIF, denoted by Δ^{199}Hg) is often used as a tracer of mercury sources in modern (Blum et al., 2014) and ancient (Grasby et al., 2019, and references therein) marine sediments. Hg(II) in pre-anthropogenic marine sediments typically shows positive MIF as a result of photoreduction in seawater (Blum et al., 2014). Δ^{199}Hg values related to volcanic and hydrothermal emissions are often within a small range near zero (0.02‰ ± 0.06‰) (Yin et al., 2016). In our study, the cross plot of Δ^{199}Hg and Δ^{201}Hg indicates that the Hg isotope fractionation was dominantly controlled by photoreduction of aqueous Hg (II) driven by natural dissolved organic matter (Fig. 5A). Δ^{199}Hg values between −0.08‰ and + 0.21‰ (average of +0.07‰), in the LM occur where both Hg concentrations and Hg/TOC are higher. More specifically, the Δ^{199}Hg values of the upper part of the LM are similar to the values of volcanic sources, which have values of 0.02‰ ± 0.06‰ (Yin et al., 2016), suggesting volcanic Hg loading at this time. The Δ^{199}Hg values of the lower part of LM are more positive, suggesting a more mixed volcanic (near zero Δ^{199}Hg value) and marine (positive Δ^{199}Hg value) source (Yin et al., 2016). In the UM, the average Δ^{199}Hg value is −0.06‰ (ranging from −0.18‰ to 0.08‰, excluding one outlier near 37 m), which are just slightly lower than that the near zero Δ^{199}Hg values of volcanic sources. The δ^{202}Hg values at this level exhibit a trend that is a mirror image of Δ^{199}Hg data (Fig. 5B), supporting that there were different sources of Hg in the LM and UM, respectively (although δ^{202}Hg could be altered by numerous biological-

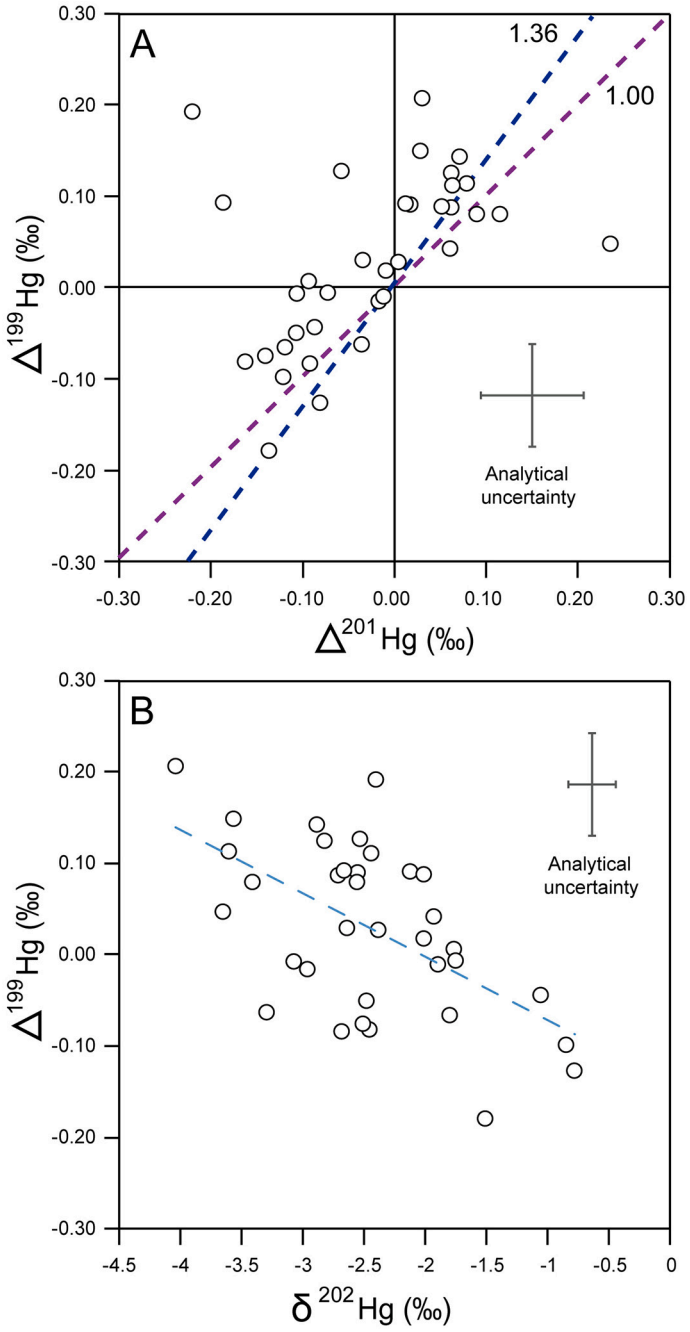

Fig. 5. Cross plots of: (A) Δ^{199}Hg and Δ^{201}Hg, and (B) Δ^{199}Hg and δ^{202}Hg. Refer to the web version for interpretation of the color.

and chemical-processes (Blum et al., 2014)).

The various Δ^{199}Hg records in the Tongren (this study) and the Zhijin (Yin et al., 2017) area support different proportions of volcanic and marine Hg sources sequestered into the lower Cambrian sediments in South China. The more positive Δ^{199}Hg values in Zhijing than in Tongren likely reflects deposition of a greater proportion of seawater-sourced Hg to the sediments, and thus reflect greater distance from any potential volcanic centers (Fig. 6). This is inconsistent with subareal LIP events that show global atmospheric distribution of Hg (e.g. Grasby et al., 2019, Shen et al., 2019a, 2019b), in contrast to submarine eruptions that show more limited Hg distribution (e.g. Percvial et al., 2018, Zhu et al., 2020). The limited volcanic signature in the lower Cambrian sediments in South China thus support submarine volcanisms (or hydrothermal fluids) near the southeast marginal of South China as the source of enhanced Hg inputs. This is also supported by higher Hg content in the southern region (e.g., Tongren, Zhijin, and Maoshi) of South China than that in more northern settings (Shatan, Luojiacun) (Fig. 1B).

Intense hydrothermal fluids released into the early Cambrian oceans of South China is also evidenced by the distribution of rare earth elements (REE) in the LM. Europium (Eu) and cerium (Ce) are the only REEs to have multiple valences, making them subject to fractionation that can be represented as Eu and Ce anomalies. Eu does not fractionate readily at Earth-surface temperatures, so Eu anomalies (Eu / Eu*) in sediments are generally inherited from source materials (Elderfield, 1988). Modern tectonic environments (i.e., the mid-Atlantic ridge and the Pacific uplift) in the deep-sea hydrothermal systems usually have similar REE concentrations and patterns (significantly positive Eu anomaly) (Douville et al., 1999). In our study, the lower Niutitang Formation shows significant positive Eu anomalies (Fig. 7, Table. 1).

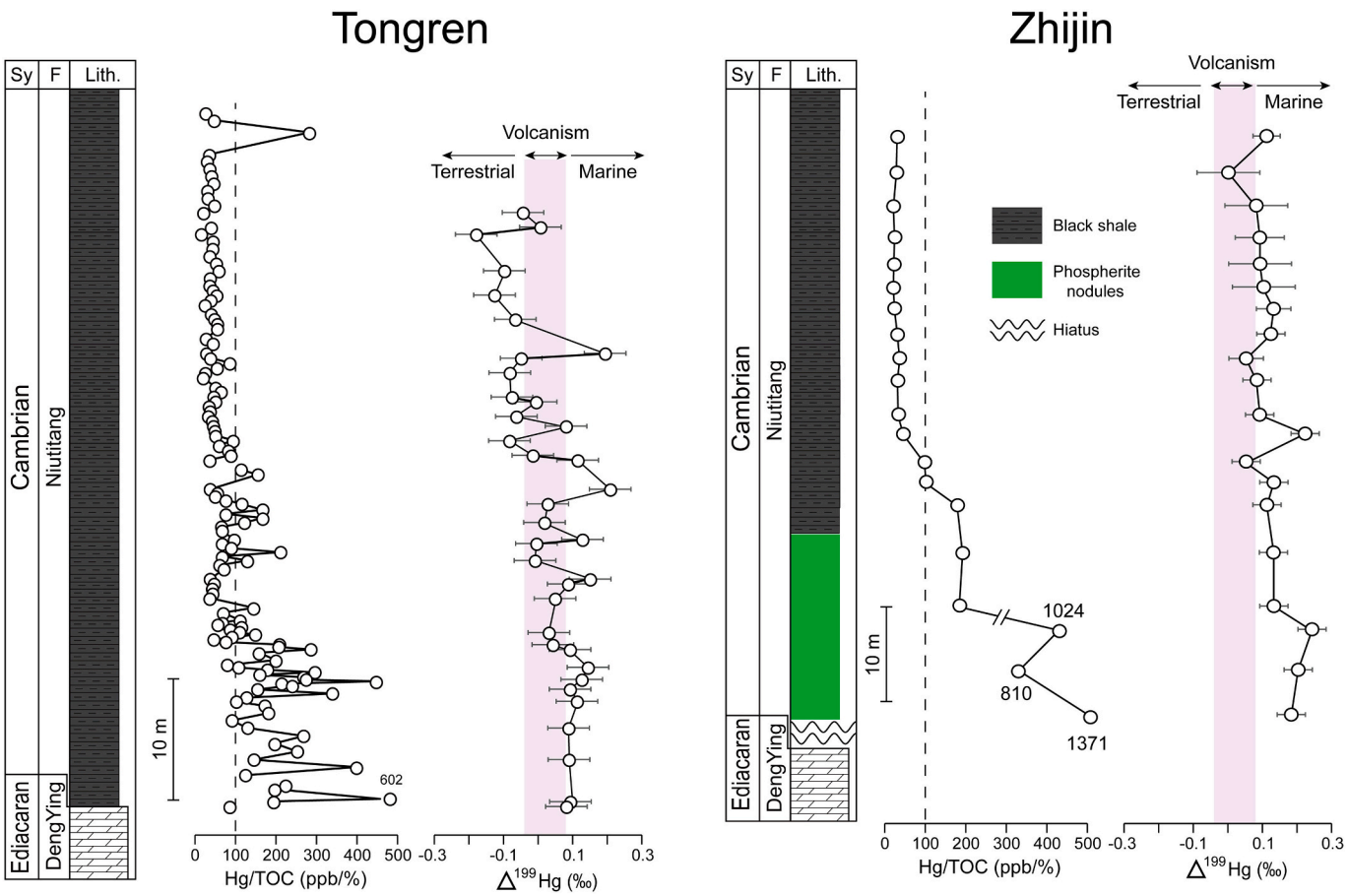

Fig. 6. Correlations of Hg/TOC and Δ^{199}Hg records for Tongren (This study) and Zhijin (Yin et al., 2017). Other details refer to Fig. 3. Refer to the web version for interpretation of the color.

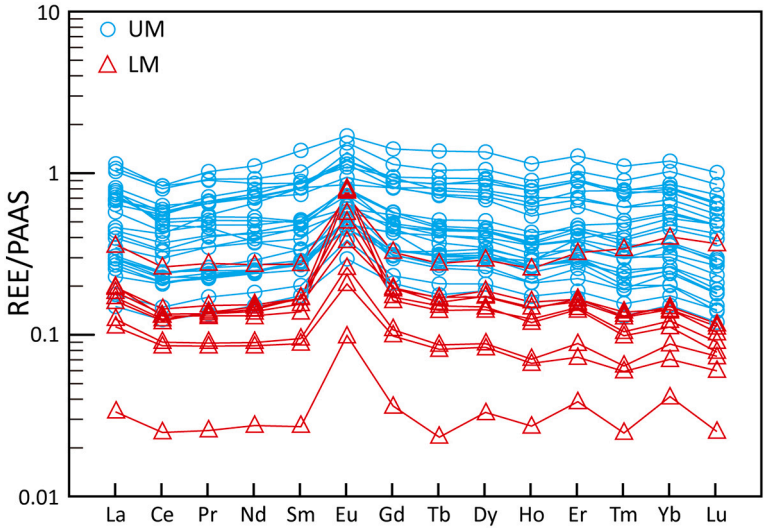

Fig. 7. PAAS-normalized rare earth elements patterns for black shales of Niutitang Formation during the early Cambrian. LM = Lower Member; UM = Upper Member. Refer to the web version for interpretation of the color.

These Eu anomalies (Eu/Eu* = 1.88, maximum = 4.96) differ from those of the contemporaneously deposited limestone (average Eu/Eu* = 1.04) (Ling et al., 2013), modern seawater (Eu/Eu* = 1.05, Alibo and Nozaki, 1999) and most black shales (Eu/Eu* < 1) (Jiang et al., 2006). In contrast, our Eu anomalies are similar to the higher Eu/Eu* values of hydrothermal fluids (Eu/Eu* = 10.6–93.0, Douville et al., 1999). In addition, these Eu anomalies also show similarities with those of polymetallic sulfide deposits (0.60–2.78) and phosphate nodules (0.92–1.39) close to the basal Niutitang Formation, which are considered to be the results of hydrothermal fluid ejected from the seafloor (Jiang et al., 2006; Zhu et al., 2014). Thus, the high Eu/Eu*values in the lower part of the Niutitang Formation may indicate that hydrothermal fluid

influenced the marine environment.

Intense hydrothermal activities were also suggested in multiple records of the early Cambrian strata in South China. Han et al. (2017) found many dolomite and organic matter debris within calcite veins in the Niutitang and Dengying formations in Guizhou and Hunan Provinces, along with syngenetic pyrite particles in dolomite debris, which are believed to indicate hydrothermal metamorphism (Han et al., 2015). Furthermore, there are abundant hydrothermal dolomite and barite-calcite veins in the dolostone of the Dengying Formation, indicating the occurrence of a variety of hydrothermal fluids, these hydrothermal processes provide the most probable contribution for polymetallic Ni-Mo-PGE mineralization (Han et al., 2017). In addition, the abundant veins in the dolomite, barite and calcite associations also indicate hydrothermal activity during this contemporaneous period. These veins may be related to the hydrothermal dolomites and dolomitization in the Niutitang and Dengying formations in Guizhou and Hunan as well as the barite deposits (Liu et al., 2014). Furthermore, large amounts of cherts deposited along the southern margin of the Yangtze Platform, which formed veins, breccia-like and layered, structures were also considered to be influenced by low-temperature silicon-rich hydrothermal systems (Chen et al., 2009).

5.4. Hydrothermal effect on the oceanic ecosystem

Hydrothermal activity was demonstrated to exist during the Ediacaran-Cambrian transition in South China, especially at the slope facies (Fig. 8, Chen et al., 2009; Han et al., 2017). Modern hydrothermal activity is known to release large amounts of highly ^{13}C-depleted greenhouse gases, H_2S, Fe, Si, and many trace elements into the oceans (e.g. Douville et al., 1999). Chen et al. (2009) proposed the area of hydrothermal vent fields in South China is about 50,000–120,000 km^2 and that the hydrothermal activity during the early Cambrian were likely of global significance. On the one hand, abundant highly ^{13}C-depleted greenhouse gases (i.e. methane) released to the ocean may lead to large-magnitude negative excursion of carbon isotopes (Chen et al., 2009). On the other hand, large amounts of nutrients (e.g., P) released from the hydrothermal vents transported to shallow water by upwelling may have led to increased palaeo-productivity (Liu et al., 2018). Abundant reduced metal elements (Fe, Mo, U) released from the hydrothermal vents could have also led to oceanic anoxia, and in turn, enhanced organic matter burial, which could have driven atmospheric and shallow water oxygenation during the early Cambrian (He et al., 2019).

Higher TOC contents in the Tongren area than other regions suggests that intense hydrothermal activity affected the local to regional environment (Fig. 9). Hydrothermal fluids bringing significant nutrients and metals to the seawater likely drove elevated productivity and/or intense reducing conditions. Local hydrothermal activity would then also drive formation of the organic matter enriched sediments in the Tongren area, which may be the main focus of shale gas exploration in China (Fig. 9).

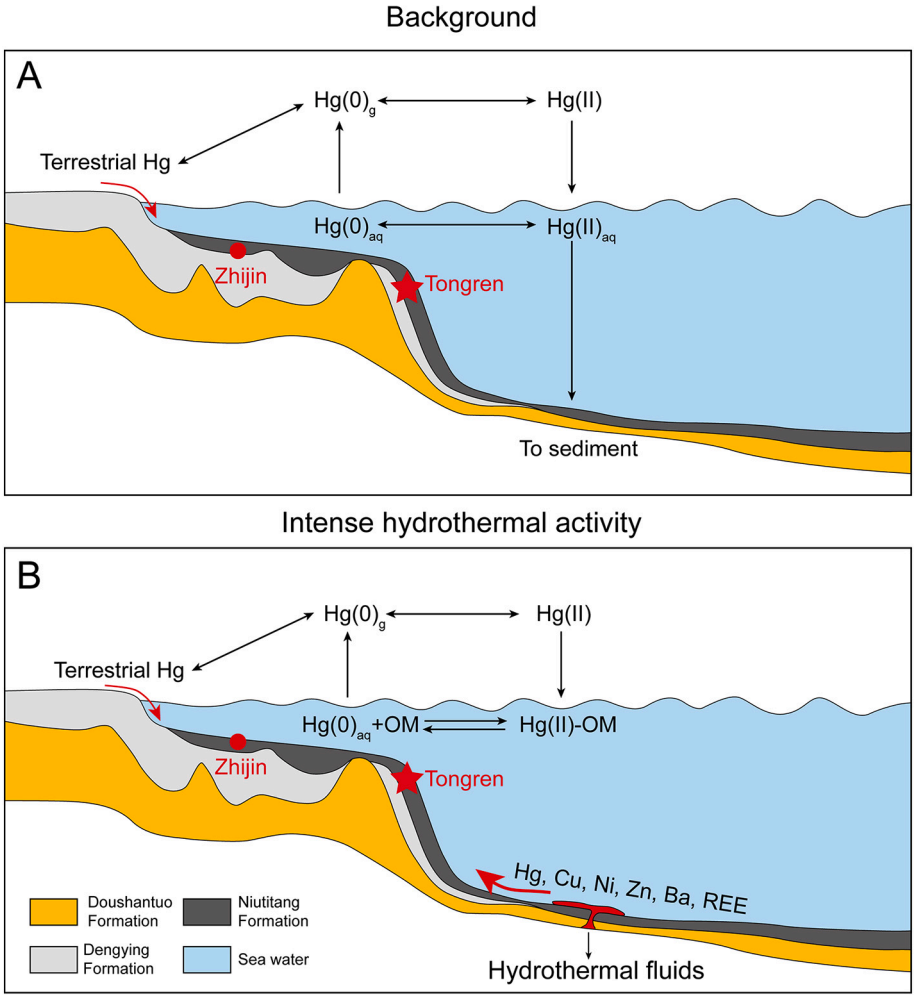

Fig. 8. Conceptual model illustrating the mechanisms of Hg contents in black shales of Niutitang Formation during the early Cambrian. (A) Normal sedimentation. (B) Sedimentation affected by hydrothermal activities. Hg(II)—OM represents the complex of Hg and organic matter. Refer to the web version for interpretation of the color.

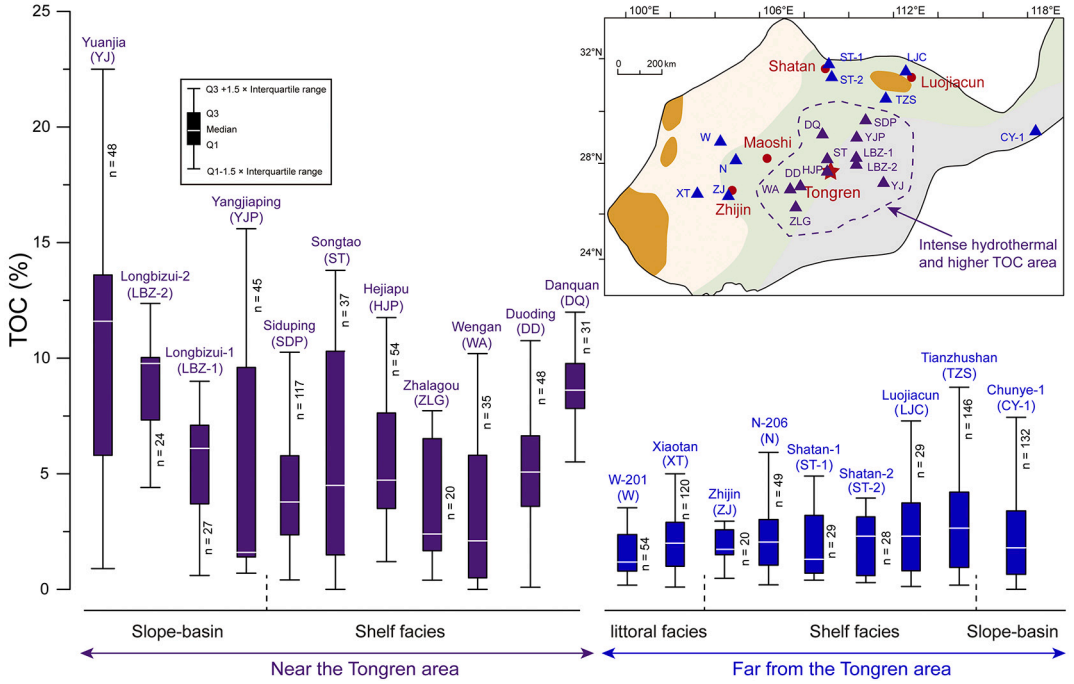

Fig. 9. Boxplot of concentrations of total organic carbon (TOC) of the early Cambrian in different settings in South China. The data used in this figure refer to supplementary materials. Refer to the web version for interpretation of the color.

Moreover, silica enriched hydrothermal fluids released to the ocean could have led to the formation of abundant bedded chert in the Liuchapo Formation (Tarasov et al., 1999; Racki and Cordey, 2000). It is also possible that such a high concentration of dissolved silica may have triggered the occurrence of siliceous organisms (i.e. siliceous sponges and radiolarians) in the lower Cambrian in South China (Ma et al., 2021).

6. Conclusions

We reported anomalous Hg concentrations in the lower Cambrian black shales and revealed that Hg in these sediments is hosted dominantly in organic matter. Elevated Hg concentrations provide direct evidence of intense hydrothermal activity during the early Cambrian in South China. Intense submarine volcanisms occurred during the deposition of the lower member of the Niutitang Formation were evidenced by elevated Hg enrichment as well as near–zero MIF values. Significant positive Eu anomalies also support intense submarine volcanism, which could be a significant source for many metal elements, and likely played a significant role in the environmental perturbations and biotic evolutions during the early Cambrian, at least in South China.

Declaration of Competing Interest

None.

Acknowledgments

This project is funded by the National Natural Science Foundation of China (42073068), China National Petroleum Corporation (CNPC) Scientific research and technology development project (Grant No.: 2019B-04, 2018A-0102).

Appendix A. Supplementary data

Supplementary data to this article can be found online at https://doi.org/10.1016/j.palaeo.2021.110294.

References

Algeo, T.J., Tribovillard, N., 2009. Environmental analysis of paleoceanographic systems based on molybdenum–uranium covariation. Chem. Geol. 268, 211–225.
Alibo, D.S., Nozaki, Y., 1999. Rare earth elements in seawater: particle association, shale-normalization, and Ce oxidation. Geochim. Cosmochim. Acta 63, 363–372.
Anbar, A.D., Knoll, A.H., 2002. Proterozoic Ocean chemistry and evolution: a bioinorganic bridge? Science 297 (5584), 1137–1142.
Baross, J.A., Hoffman, S.E., 1985. Submarine hydrothermal vents and associated gradient environment as sites for the origin and evolution of life. Orig. Life Evol. Biosph. 15, 327–345.
Blum, J.D., Sherman, L.S., Johnson, M.W., 2014. Mercury isotopes in earth and environmental sciences. Annu. Rev. of Earth Planet Sci. 42, 249–269.
Chen, D.Z., Wang, J.G., Qing, H.R., Yan, D.T., Li, R.W., 2009. Hydrothermal venting activities in the early Cambrian, South China: petrological, geochronological and stable isotopic constraints. Chem. Geol. 258, 168–181.
Chen, D.Z., Zhou, X.Q., Fu, Y., Wang, J.G., Yan, D.T., 2015. New U–Pb zircon ages of the Ediacaran–Cambrian boundary strata in South China. Terra Nova 27, 62–68.
Douville, E., Bienvenu, P., Charlou, J.L., Donval, J.P., Fouquet, Y., Appriou, P., Gamo, T., 1999. Yttrium and rare earth elements in fluids from various deep-sea hydrothermal systems. Geochim. Cosmochim. Acta 63, 627–643.
Faggetter, L., Wignall, P.B., Pruss, S.B., Jones, D.S., Grasby, S.E., Widdowson, M., Newton, R.J., 2019. Mercury chemostratigraphy across the Cambrian Series 2 – Series 3 boundary: evidence for increased volcanic activity coincident with extinction? Chem. Geol. 510, 188–199.
Grasby, S.E., Shen, W., Yin, R., Gleason, J.D., Blum, J.D., Lepak, R.F., Hurley, J.P., Beauchamp, B., 2017. Isotopic signatures of mercury contamination in latest Permian oceans. Geology 45, 55–58.
Grasby, S.E., Them, T.R., Chen, Z., Yin, R., Ardakani, O.H., 2019. Mercury as a proxy for volcanic emissions in the geologic record. Earth-Sci. Rev. 196, 102880.
Grasby, S.E., Liu, X., Yin, R., Ernst, R.E., Chen, Z., 2020. Toxic mercury pulses into late Permian terrestrial and marine environments. Geology 48, 830–833.
Guo, Q.J., Deng, Y.N., Hippler, D., Franz, G., Zhang, J.M., 2016. REE and trace element patterns from organic-rich rocks of the Ediacaran-Cambrian transitional interval. Gondwana Res. 36, 81–93.
Han, T., Zhu, X.Q., Li, K., Jiang, L., Zhao, C.H., Wang, Z.G., 2015. Metal sources for the polymetallic Ni–Mo–PGE mineralization in the black shales of the lower Cambrian Niutitang Formation, South China. Ore Geol. Rev. 67, 158–169.
Han, T., Fan, H.F., Zhu, X.Q., Wen, H.J., Zhao, C.H., Xiao, F., 2017. Submarine hydrothermal contribution for the extreme element accumulation during the early Cambrian, South China. Ore Geol. Rev. 86, 297–308.
He, T.C., Zhu, M.Y., Mills, B.J.W., Wynn, P.M., Zhuravlev, A.Y., Tostevin, R., von Strandmann, P.A.E.P., Yang, A.H., Poulton, S.W., Shields, G.A., 2019. Possible links between extreme oxygen perturbations and the Cambrian radiation of animals. Nat. Geosci. 12, 468–474.
Huang, Q., Chen, J.B., Huang, W.L., 2016. Isotope composition for source identification of mercury in atmospheric fine particles. Atmos. Chem. Phys. 16, 11773–11786.

Jiang, G.Q., Wang, X.Q., Shi, X.Y., Xiao, S.H., Zhang, S.H., Dong, J., 2012. The origin of decoupled carbonate and organic carbon isotope signatures in the early Cambrian (ca. 542–520 Ma) Yangtze platform. Earth Planet. Sci. Lett. 317–318, 96–110.
Jiang, S.Y., Chen, Y.Q., Ling, H.F., Yang, J.H., Feng, H.Z., Ni, P., 2006. Trace and rare earth element geochemistry and Pb–Pb dating of black shales and intercalated Ni–Mo–PGE–Au sulfide ores in lower Cambrian strata, Yangtze Platform, South China. Mineral. Deposita 41, 453–467.
Jin, C.S., Li, C., Algeo, T.J., Planavsky, N.J., Cui, H., Yang, X.L., Zhao, Y.L., Zhang, X.L., Xie, S.C., 2016. A highly redox-heterogeneous ocean in South China during the early Cambrian (529–514 Ma): implications for biota-environment co-evolution. Earth Planet. Sci. Lett. 441, 38–51.
Knoll, A.H., Carroll, S.B., 1999. Early animal evolution: emerging views from comparative biology and geology. Science 284 (5423), 2129–2137.
Lehmann, B., Nagler, T.F., Holland, H.D., Wille, M., Mao, J.W., Pan, J.Y., Ma, D.S., Dulski, P., 2007. Highly metalliferous carbonaceous shale and early Cambrian seawater. Geology 35, 403–406.
Li, C., Jin, C.S., Planavsky, N.J., Algeo, T.J., Cheng, M., Yang, X.L., Zhao, Y.L., Xie, S.C., 2017. Coupled oceanic oxygenation and metazoan diversification during the early-middle Cambrian? Geology. 45 (8), 743–746.
Li, Z.-X., Bogdanova, S., Collins, A., Davidson, A., De Waele, B., Ernst, R., Fitzsimons, I., Fuck, R., Gladkochub, D., Jacobs, J., 2008. Assembly, configuration, and break-up history of Rodinia: a synthesis. Precambrian Res. 160, 179–210.
Ling, H.F., Chen, X., Li, D., Wang, D., Shields-Zhou, G.A., Zhu, M.Y., 2013. Cerium anomaly variations in Ediacaran–earliest Cambrian carbonates from the Yangtze Gorges area, South China: implications for oxygenation of coeval shallow seawater. Precambrian Res. 225, 110–127.
Liu, K., Feng, Q.L., Shen, J., Khan, M., Planavsky, N.J., 2018. Increased productivity as a primary driver of marine anoxia in the lower Cambrian. Palaeogeogr. Palaeoclimatol. Palaeoecol. 491, 1–9.
Liu, S.G., Huang, W.M., Jansa, L.F., Wang, G.Z., Song, G.Y., Zhang, C.J., Sun, W., Ma, W. X., 2014. Hydrothermal dolomite in the upper Sinian (upper Proterozoic) Dengying Formation, east Sichuan Basin, China. Acta Geol. Sin. 88, 1466–1487 (English Edition).
Mcdermott, J.M., Seewald, J.S., German, C.R., Sylva, S.P., 2015. Pathways for abiotic organic synthesis at submarine hydrothermal fields. Proc. Natl. Acad. Sci. U. S. A. 112, 7668–7672.
Narbonne, G.M., 2005. The Ediacara biota: Neoproterozoic origin of animals and their ecosystems. Annu. Rev. Earth Planet Sci. 33, 421–442.
Och, L.M., Cremonese, L., Shields-Zhou, G.A., Poulton, S.W., Struck, U., Ling, H.F., Li, D., Chen, X., Manning, C., Thirlwall, M., Strauss, H., Zhu, M., 2015. Palaeoceanographic controls on spatial redox distribution over the Yangtze Platform during the Ediacaran-Cambrian transition. Sedimentology. 63, 378–410.
Perner, M., Hansen, M., Seifert, R., Strauss, H., Koschinsky, A., Petersen, S., 2013. Linking geology, fluid chemistry, and microbial activity of basalt and ultramafic-hosted deep-sea hydrothermal vent environments. Geobiology 11, 340–355.
Ravichandran, M., 2004. Interactions between mercury and dissolved organic matter—a review. Chemosphere 55 (3), 319–331.
Sanei, H., Grasby, S.E., Beauchamp, B., 2012. Latest Permian mercury anomalies. Geology 40 (1), 63–66.
Selin, N.E., 2009. Global biogeochemical cycling of mercury: a review. Annu. Rev. Environ. Resour. 34, 43–63.
Shen, J., Algeo, T.J., Chen, J.B., Planavsky, N.J., Feng, Q.L., Yu, J.X., Liu, J.L., 2019a. Mercury in marine Ordovician-Silurian boundary sections of South China is sulfide-hosted and non-volcanic in origin. Earth Planet. Sci. Lett. 511, 130–140.
Shen, J., Chen, J.B., Algeo, T.J., Yuan, S.L., Feng, Q.L., Yu, J.X., Zhou, L., O'Connell, B., Planavsky, N.J., 2019b. Evidence for a prolonged Permian-Triassic extinction interval from global marine mercury records. Nat. Commun. 10, 1563.
Shen, J., Feng, Q.L., Algeo, T.J., Liu, J.L., Zhou, C.Y., Wei, W., Liu, J.S., Them, T.R., Gill, B.C., Chen, J.B., 2020. Sedimentary host phases of mercury (Hg) and implications for use of Hg as a volcanic proxy. Earth Planet. Sci. Lett. 543, 116333.
Shu, D.G., Isozaki, Y., Zhang, X.L., Han, J., Isozaki, S., 2014. Birth and early evolution of metazoans. Gondwana Res. 25, 884–895.
Steiner, M., Li, G., Qian, Y., Zhu, M., Erdtmann, B.D., 2007. Neoproterozoic to early Cambrian small shelly fossil assemblages and a revised biostrati-graphic correlation of the Yangtze Platform (China). Palaeogeogr. Palaeoclimatol. Palaeoecol. 254, 67–99.
Taylor, S.R., Mclennan, S.M., 1985. The Continental Crust: Its Composition and Evolution. Blackwell, Oxford (312).
Them, T.R., Jagoe, C.H., Caruthers, A.H., Gill, B.C., Grasby, S.E., Gröcke, D.R., Yin, R., 2019. Terrestrial sources as the primary delivery mechanism of mercury to the oceans across the Toarcian Oceanic Anoxic Event (early Jurassic). Earth Planet. Sci. Lett. 507, 62–72.
Wang, H.Z., 1985. Atlas of the Paleogeography of China. Cartographic Publishing House, Beijing (283). (in Chinese).
Yin, R.S., Feng, X.B., Hurley, J.P., Krabbenhoft, D.P., Lepak, R.F., Hu, R.Z., Zhang, Q., Li, Z.G., Bi, X.W., 2016. Mercury isotopes as proxies to identify sources and environmental impacts of mercury in sphalerites. Sci. Rep. 6, 18686.
Yin, R.S., Xu, L.G., Lehmann, B., Lepak, R.F., Hurley, J.P., Mao, J.W., Feng, X.B., Hu, R. Z., 2017. Anomalous mercury enrichment in early Cambrian black shales of South China: Mercury isotopes indicate a seawater source. Chem. Geol. 467, 159–167.
Zheng, W., Hintelmann, H., 2010. Isotope fractionation of mercury during its photochemical reduction by low-molecular-weight organic compounds. J. Phys. Chem. A 114, 4246–4253.
Zhou, C.M., Jiang, S.Y., 2009. Palaeoceanographic redox environments for the lower Cambrian Hetang Formation in South China: evidence from pyrite framboids, redox sensitive trace elements, and sponge biota occurrence. Palaeogeogr. Palaeoclimatol. Palaeoecol. 271, 279–286.
Zhu, B., Jiang, S.Y., Yang, J.H., Pi, D.H., Ling, H.F., Chen, Y.Q., 2014. Rare earth element and Sr-Nd isotope geochemistry of phosphate nodules from the lower Cambrian Niutitang Formation, NW Hunan Province. South China. Palaeogeogr. Palaeoclimatol. Palaeoecol. 398, 132–143.
Zhu, C.W., Tao, C.H., Yin, R.S., Liao, S.L., Yang, W.F., Liu, J., Barriga, F.J.A.S., 2020. Seawater versus mantle sources of mercury in sulfide-rich seafloor hydrothermal systems, Southwest Indian Ridge. Geochim. Cosmochim. Acta 281, 91–101.
Zhu, G.Y., Wang, T.S., Xie, Z.Y., Xie, B.H., Liu, K.Y., 2015. Giant gas discovery in the Precambrian deeply buried reservoirs in the Sichuan Basin, China: implications for gas exploration in old cratonic basins. Precambrian Res. 262, 45–66.
Zhu, M.Y., 2010. The origin and Cambrian explosion of animals: fossil evidences from China. Acta Palaeontol. Sin. 49 (3), 269–287 (in Chinese with English abstract).